

# Optimally robust shortcuts to population inversion in cat-state qubits

Shao-Wei Xu,<sup>1</sup> Zhong-Zheng Zhang,<sup>1</sup> Yue-Ying Guo,<sup>1</sup> Ye-Hong Chen,<sup>1,2,3,\*</sup> and Yan Xia<sup>1,2</sup>

<sup>1</sup>*Department of Physics, Fuzhou University, Fuzhou 350116, China*

<sup>2</sup>*Fujian Key Laboratory of Quantum Information and Quantum Optics, Fuzhou University, Fuzhou 350116, China*

<sup>3</sup>*Theoretical Quantum Physics Laboratory, RIKEN Cluster for Pioneering Research, Wako-shi, Saitama 351-0198, Japan*

(Dated: August 2, 2024)

Cat-state qubits formed by photonic coherent states are a promising candidate for realizing fault-tolerant quantum computing. Such logic qubits have a biased noise channel that the bit-flip error dominates over all the other errors. In this manuscript, we propose an optimally robust protocol using the control method of shortcuts to adiabaticity to realize a nearly perfect population inversion in a cat-state qubit. We construct a shortcut based on the Lewis-Riesenfeld invariant and examine the stability versus different types of perturbations for the fast and robust population inversion. Numerical simulations demonstrate that the population inversion can be mostly insensitive to systematic errors in our protocol. Even when the parameter imperfection rate for bit-flip control is 20%, the final population of the target state can still reach  $\geq 99\%$ . The optimally robust control provides a feasible method for fault-tolerant and scalable quantum computation.

## I. INTRODUCTION

Quantum computers promise to drastically outperform classical computers on certain problems, such as factoring, (approximate) optimization, boson sampling, or unstructured database searching [1–5]. Building a large-scale quantum computer requires qubits that can be protected from errors, i.e., utilizing quantum error correction. During the past decades, many strategies using physical and logical qubits for quantum error correction have been developed. Noting that quantum error correction with physical qubits usually requires huge physical resource overhead, this makes it difficult to scale up the number of qubits for a large-scale quantum computer [6–12]. This is why in recent years, much attention has been paid to logic qubits formed by bosonic codes [11–16], which allow quantum error correction extending only the number of excitation instead of the number of qubits.

A promising alternative with the potential to realize quantum error correction beyond the break-even point involves encoding logical qubits in continuous variables [14, 15, 17–23], such as coherent states. This gives rise to the cat-state codes, which are formed by even and odd coherent states of a single optical mode [14, 15, 18–22, 24–26]. The cat-state qubits preserve the noise bias that experience only bit-flip noise, reducing the number of building blocks of layers for error correction [15, 18–20, 26]. Moreover, the first experiment [27] realizing cat-state qubits showed a strong suppression of frequency fluctuations due to  $1/f$  noise [27–30]. All these make the cat-state qubits promising for hardware efficient universal quantum computing.

In an implementation of quantum computation, high-fidelity single- and two-qubit quantum gates are essential elements of quantum computation because

quantum algorithms are usually designed as a sequence of such simple quantum gates [5, 29]. Though several experiments have realized the control of cat-state qubits [27, 31], the robust control of a single cat-state qubit is still a problem to be solved. In this manuscript, we propose an optimally robust shortcuts to adiabatic protocol for controlling a cat-state qubit. Shortcuts to adiabaticity [24, 32–42] are a series of protocols mimicking adiabatic dynamics beyond the adiabatic limit and have been widely applied for quantum state engineering. One of the more prominent of these protocols is the method of “invariant-based reverse engineering” [43, 44], which can construct shortcuts only by redesigning system parameters without destroying the initial form of the system Hamiltonian. This provides an alternative control method for the cat-state qubits with large amplitudes because such qubits can be manipulated along only one direction on the Bloch sphere [19]. Moreover, the invariant-based reverse engineering is compatible with various quantum optimized control techniques [45]. One can thus optimize the parameters to realize a high-fidelity population inversion of a cat-state qubit.

This manuscript is organized as follows. In Sec. II, we present the model and the effective Hamiltonian for the protocol. The protocol of constructing shortcuts to adiabatic passage is given in Sec. III. In Sec. IV, we analyze the systemic error sensitivity of the cat-state qubit. Then, in Sec. V the optimal protocol to minimize the systemic error sensitivity is presented. Moreover, we discuss the influence of single-photon loss and pure dephasing on the protocol in Sec. VI. Finally, the conclusions are given in Sec. VII.

## II. MODEL AND EFFECTIVE HAMILTONIAN

Considering that a Kerr-nonlinear resonator with frequency  $\omega_c$  is driven by a single-mode, two-photon excitation, where the driving frequency for the two-photon

---

\* yehong.chen@fzu.edu.cn

excitation is twice the resonator frequency. In the rotating-wave approximation, the system Hamiltonian is given by (hereafter  $\hbar = 1$ )

$$H_{\text{Kerr}} = -Ka^{\dagger 2}a^2 + P(a^{\dagger 2} + a^2). \quad (1)$$

In the above expression,  $a$  and  $a^\dagger$  are the annihilation and creation operators for photons,  $K$  is the strength of the Kerr-nonlinearity, and  $P$  is the strength of the two-photon drive.

We can observe that Eq. (1) is written in the rotating frame. In this frame, the simplified Hamiltonian is described as having quasi-energy eigenstates with negative energies. Specifically, by applying the displacement transformation  $D(\pm\alpha) = \exp[\pm\alpha(a^\dagger - a)]$  to  $H_{\text{Kerr}}$ , the Hamiltonian in Eq. (1) becomes

$$\begin{aligned} H' &= D(\pm\alpha)H_{\text{Kerr}}D^\dagger(\pm\alpha) \\ &= -4K\alpha^2a^\dagger a - Ka^{\dagger 2}a^2 \mp 2K\alpha(a^{\dagger 2}a + \text{H.c.}), \end{aligned} \quad (2)$$

where  $\alpha = \sqrt{\frac{P}{K}}$ . The vacuum  $|0\rangle$  is exactly an eigenstate of  $H'$ . Therefore, the coherent states  $D(\pm\alpha)|0\rangle = |\pm\alpha\rangle$  or, equivalently, their superposition states

$$|\mathcal{C}_\pm\rangle = \mathcal{N}_\pm(|\alpha\rangle \pm |-\alpha\rangle), \quad (3)$$

are the degenerate eigenstates of  $H_{\text{Kerr}}$ , where  $\mathcal{N}_\pm = 1/\sqrt{2(1 \pm e^{-2|\alpha|^2})}$  are normalized coefficients. In the limit of large  $\alpha$ , one can obtain  $\alpha^2 \gg \alpha^1, \alpha^0$ . Thus, Eq. (2) is approximated by  $H' \simeq -4K\alpha^2a^\dagger a$ , which is the Hamiltonian of a (inverted) harmonic oscillator. Therefore, in the original frame, the eigenstates of  $H_{\text{Kerr}}$  are eigenstates of the parity operator (see Fig. 1). The first-excited states can be approximately expressed as two orthogonal states  $|\psi_\pm^{e,1}\rangle = \mathcal{N}_\pm^{e,1}[D(\alpha) \pm D(-\alpha)]|n=1\rangle$ , where  $\mathcal{N}_\pm^{e,1}$  are normalized coefficients and  $|n\rangle$  are Fock states. The energy gap between the cat states subspace  $\mathcal{C}$  and  $|\psi_\pm^{e,1}\rangle$  can be approximated as  $\omega_{\text{gap}} \simeq 4K\alpha^2$ .

As shown in Fig. 1, the cat states subspace  $\mathcal{C}$  is separated from the rest of the Hilbert space  $\mathcal{C}_\perp$  by an energy gap of approximately  $\omega_{\text{gap}} \simeq 4K\alpha^2$ . In the limit of large  $\alpha$ , the action of  $a$  can only flip the two cat states  $|\mathcal{C}_\pm\rangle$ , i.e.,

$$a|\mathcal{C}_\pm\rangle \simeq \alpha|\mathcal{C}_\mp\rangle. \quad (4)$$

Now, in the interaction picture, we add a control Hamiltonian [46]

$$\begin{aligned} H_c(t) &= -\frac{E_J(t)}{2} \{D[i\varphi_a \exp(i\omega_c t)] + \text{H.c.}\} \\ &\quad + \epsilon(t)(a^\dagger + a). \end{aligned} \quad (5)$$

A possible implementation of this control Hamiltonian is the superconducting circuits [46] by considering the Kerr-nonlinearity mode coupled capacitively to a Josephson junction and assuming that other modes (including

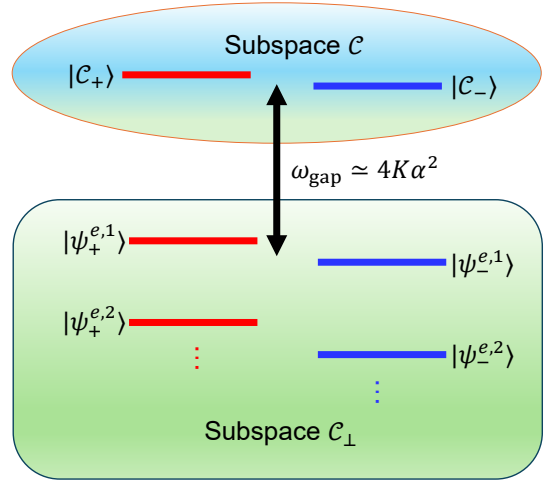


FIG. 1. In the rotating frame determined by Eq. (2), the characteristic spectrum of the Kerr-nonlinearity resonator  $H_{\text{Kerr}}$ .

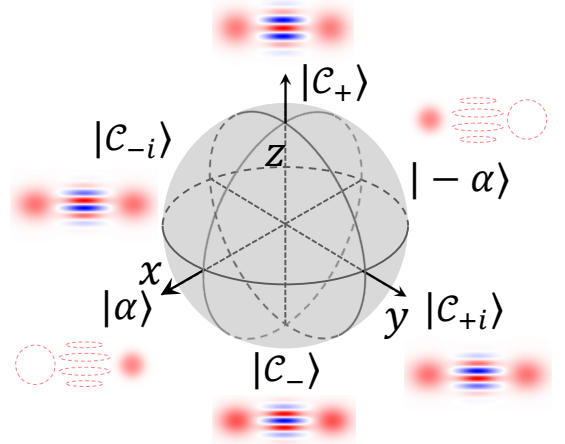


FIG. 2. Bloch sphere of the cat-state qubit described by Eq. (10) when  $\alpha = 2$ . For simplicity, we assume  $\alpha = 2$  throughout the manuscript.

the junction mode) are never excited. Accordingly, the time-dependent parameter  $E_J(t)$  is the effective Josephson energy and  $\varphi_a$  is the phase. A single photon driving with time-dependent amplitude  $\epsilon(t)$  is also applied to the system. For  $E_J(t), \epsilon(t) \ll \omega_c$ , the effective Hamiltonian under the rotating-wave approximation becomes

$$H'_c(t) = E_J e^{-\varphi_a^2/2} \sum_{m=0}^{\infty} L_m(\varphi_a^2) |n\rangle\langle n| + \epsilon(a^\dagger + a), \quad (6)$$

where  $L_m(*)$  is the Laguerre polynomial of order  $m$ . Hereafter, for simplicity, we omit the explicit time dependence of parameters, e.g.,  $E_J(t) \rightarrow E_J$  and  $\epsilon(t) \rightarrow \epsilon$ .

The total Hamiltonian now becomes  $H(t) = H_{\text{Kerr}} + H'_c(t)$ . We can use the cat states  $|\mathcal{C}_\pm\rangle$  to define the Pauli

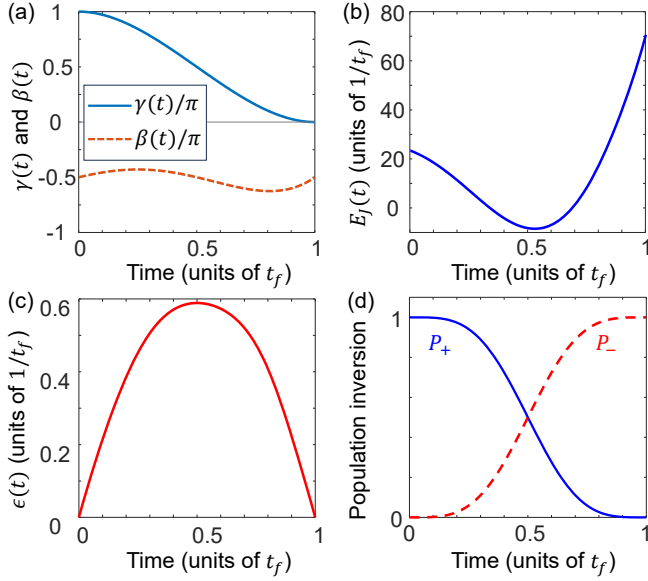


FIG. 3. (a) Polynomials  $\gamma(t) = \sum_{i=0}^3 a_i t^i$  (solid-blue curve) and  $\beta(t) = \sum_{i=0}^4 b_i t^i$  (dashed-orange curve). (b) Corresponding function of  $E_J$  calculated by  $\Delta$  in Eq. (17). (c) Corresponding function of  $\epsilon$  calculated by  $\Omega_R$  in Eq. (17). (d) Non-adiabatic population inversion in the cat-state qubit. We choose  $t_f = 5/K$  to satisfy the condition  $E_J, \epsilon \ll \omega_{\text{gap}}$ .

matrices,

$$\begin{aligned} \sigma_x &= \sigma_+ + \sigma_-, \\ \sigma_y &= i(\sigma_- - \sigma_+), \\ \sigma_z &= \sigma_+ \sigma_- - \sigma_- \sigma_+, \end{aligned} \quad (7)$$

where  $\sigma_+ = |\mathcal{C}_+\rangle\langle\mathcal{C}_-|$  is the raising operator and  $\sigma_- = |\mathcal{C}_-\rangle\langle\mathcal{C}_+|$  is the lowering operator. When

$$E_J, \epsilon \ll \omega_{\text{gap}}, \quad (8)$$

the evolution of the system can be restricted to the cat-state subspace  $\mathcal{C}$ , i.e., constructing a cat-state qubit as shown in Fig. 2. Projecting the system onto the cat-state subspace, the effective Hamiltonian  $H'_c(t)$  can be represented as

$$H_{\text{eff}} = \frac{E_J \exp[-(\varphi_a - 2\alpha)^2/2]}{-2\sqrt{\pi}\alpha\varphi_a} \sigma_z + \epsilon(\alpha^* + \alpha)\sigma_x. \quad (9)$$

We can choose  $\varphi_a = 2\alpha$  and rewrite the effective Hamiltonian in the matrix form as

$$H_{\text{eff}} = \frac{1}{2} \begin{pmatrix} \Delta & \Omega_R \\ \Omega_R & -\Delta \end{pmatrix}, \quad (10)$$

where the time-dependent parameters are  $\Delta = -E_J/(\alpha\sqrt{2\pi})$  and  $\Omega_R = 2(\alpha^* + \alpha)\epsilon$ .

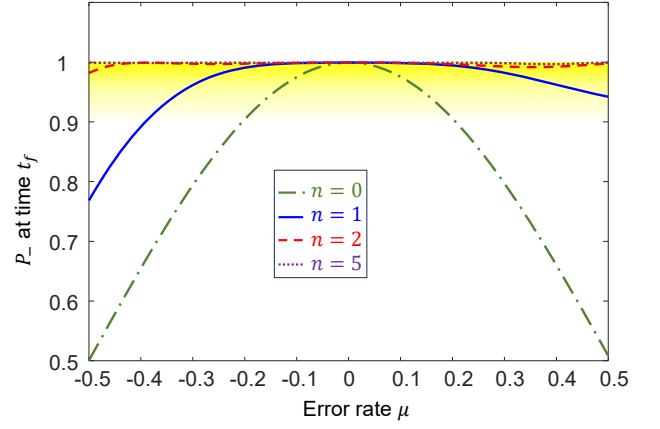


FIG. 4. Population of the odd cat state  $|\mathcal{C}_-\rangle$  at time  $t_f$  versus error rate  $\mu$  for different control parameters. The result of the protocol from Sec. III is represented by the green dashed-dotted curve, and the results of the optimal protocol in Sec. V is represented by the other curves.

### III. NON-ADIABATIC EVOLUTION BASED ON THE LEWIS-RIESENFELD INVARIANTS

Following the method of invariant-based reverse engineering [43, 44], we introduce a dynamical invariant  $I(t)$ , which satisfies

$$i \frac{\partial}{\partial t} I(t) - [H_{\text{eff}}(t), I(t)] = 0. \quad (11)$$

Then, the solution of the time-dependent Schrödinger equation

$$i \frac{\partial}{\partial t} |\psi(t)\rangle = H_{\text{eff}}(t) |\psi(t)\rangle, \quad (12)$$

can be expressed by a superposition of the eigenstates  $|\phi_n(t)\rangle$  of  $I(t)$  as

$$|\psi(t)\rangle = \sum_n c_n \psi_n(t). \quad (13)$$

Here,  $\psi_n(t) = e^{iR_n(t)} |\phi_n(t)\rangle$  and  $c_n$  are time-independent amplitudes determined by the initial state, and  $R_n(t)$  are the Lewis-Riesenfeld phases defined as

$$R_n(t) = \int_0^t \langle \phi_n(t') | i \frac{\partial}{\partial t'} - H_{\text{eff}}(t') | \phi_n(t') \rangle dt'. \quad (14)$$

Following the previous researches [32, 44, 45], for the Hamiltonian in Eq. (10), the invariant  $I(t)$  can be given by

$$I(t) = \frac{1}{2} \begin{pmatrix} \cos \gamma & \sin \gamma e^{i\beta} \\ \sin \gamma e^{-i\beta} & -\cos \gamma \end{pmatrix}, \quad (15)$$

where  $\gamma$  and  $\beta$  are two time-dependent dimensionless parameters to be determined later. The eigenstates of

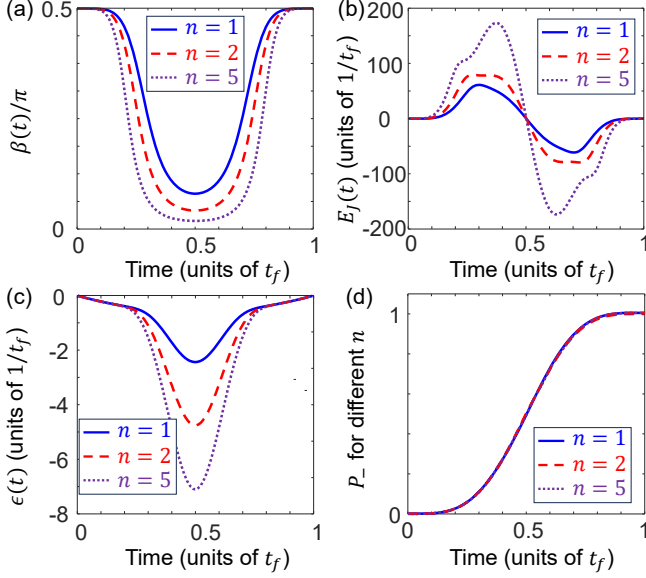


FIG. 5. (a) Parameter  $\beta$  calculated according to Eq. (37) with the polynomial  $\gamma(t) = \sum_{i=0}^3 a_i t^i$ . (b) Corresponding function of  $E_J$  calculated by  $\Delta$  in Eq. (36). (c) Corresponding function of  $\epsilon$  calculated by  $\Omega_R$  in Eq. (36). (d) Time evolution of the odd cat state  $|C_-\rangle$  for different  $n$ . The total evolution time is assumed to be  $t_f = 5/K$ .

the Lewis-Riesenfeld invariant  $I(t)$  can be thus derived as [44]

$$|\phi_+(t)\rangle = \cos\left(\frac{\gamma}{2}\right)e^{i\beta}|C_-\rangle + \sin\left(\frac{\gamma}{2}\right)|C_+\rangle,$$

$$|\phi_-(t)\rangle = \sin\left(\frac{\gamma}{2}\right)|C_-\rangle - \cos\left(\frac{\gamma}{2}\right)e^{-i\beta}|C_+\rangle. \quad (16)$$

According to Eq. (11), we obtain the expressions of the time-dependent parameters  $\Omega_R$  and  $\Delta$  as

$$\Omega_R = \dot{\gamma}/\sin\beta,$$

$$\Delta = \Omega_R \cot\gamma \cos\beta - \dot{\beta}. \quad (17)$$

To achieve the flipping of the cat states  $|C_\pm\rangle$ , one needs to set the boundary conditions  $\Omega_R(0) = \Omega_R(t_f) = 0$ , and

$$\begin{aligned} \gamma(0) &= \pi, & \gamma(t_f) &= 0, \\ \dot{\gamma}(0) &= 0, & \dot{\gamma}(t_f) &= 0. \end{aligned} \quad (18)$$

We can arbitrarily choose the values of  $\beta(0)$  and  $\beta(t_f)$ , according to Eq. (17), when  $\beta$  approaches  $(n+1/2)\pi$ , the resulting of  $|\Omega_R|$  is minimized, imposing

$$\begin{aligned} \beta(0) &= -\pi/2, & \beta(t_f/2) &= -\pi/2, & \beta(t_f) &= -\pi/2, \\ \dot{\beta}(0) &= \pi/(2t_f), & \dot{\beta}(t_f) &= \pi/(2t_f). \end{aligned} \quad (19)$$

To satisfy the boundary conditions given in Eqs. (18) and (19), we can assume

$$\gamma(t) = \sum_{i=0}^3 a_i t^i, \quad \text{and} \quad \beta(t) = \sum_{i=0}^4 b_i t^i, \quad (20)$$

and thus determine their values as shown in Fig. 3(a). Accordingly, we can obtain  $E_J$  and  $\epsilon$  [see Fig. 3(b) and Fig. 3(c)]. Such parameters allow a population inversion from the even cat state  $|C_+\rangle$  to the odd cat state  $|C_-\rangle$  through a nonadiabatic passage. This is determined by solving the Schrödinger equation  $i|\dot{\psi}(t)\rangle = H|\psi(t)\rangle$  of the total Hamiltonian

$$H = H_{\text{Kerr}} + H_c(t). \quad (21)$$

In Fig. 3(d), we display the dynamical evolution of the system when the initial state is  $|C_+\rangle$ . An almost perfect population inversion ( $P_- \simeq 99.9\%$  at  $t = t_f$ ) is obtained as shown in the figure, where the populations of the states  $|C_+\rangle$  and  $|C_-\rangle$  are defined as

$$P_\pm(t) = |\langle C_\pm | \psi(t) \rangle|^2. \quad (22)$$

#### IV. SYSTEMATIC ERROR SENSITIVITY

Now, we consider the influence of systematic errors on the system dynamics. The ideal undisturbed Hamiltonian is  $H_{\text{eff}}$ . For systematic errors, the Hamiltonian in actual experiments becomes  $H_{01} = H_0 + \mu H_1$ , which also satisfies the Schrödinger equation

$$i \frac{d}{dt} |\psi(t)\rangle = (H_0 + \mu H_1) |\psi(t)\rangle, \quad (23)$$

where  $H_0 = H_{\text{eff}}$ , and  $H_1$  is the disturbed Hamiltonian. For simplicity, we assume that errors affect the pulse amplitude but not the detuning. The disturbed Hamiltonian  $H_1$  under this assumption is

$$H_1 = \epsilon(\alpha^* + \alpha)\sigma_x. \quad (24)$$

In the original control Hamiltonian  $H_c$ , this disturbed Hamiltonian corresponds to parameter deviations in the single-photon drive  $\epsilon(a + a^\dagger)$ . Then, we define the systematic error sensitivity as

$$q_s = -\frac{1}{2} \frac{\partial^2 P_-^2}{\partial \mu^2} \Big|_{\mu=0} = -\frac{\partial P_-}{\partial (\mu^2)} \Big|_{\mu=0}, \quad (25)$$

where  $P_-$  is the population of the state  $|C_-\rangle$  at the final time  $t_f$ .

Using perturbation theory up to  $O(\mu^2)$ , we obtain

$$|\psi(t_f)\rangle = |\psi_0(t_f)\rangle - i\mu \int_0^{t_f} dt U_0(t_f, t) H_1(t) |\psi_0(t)\rangle + \dots, \quad (26)$$

where  $|\psi_0(t_f)\rangle$  is the solution without perturbation, and  $U_0(t_f, t)$  is the unperturbed time evolution operator. We assume that the protocol without errors ( $\mu = 0$ ) works perfectly, i.e.  $|\psi(t_f)\rangle = |\phi_+(t_f)\rangle = e^{i\beta(t_f)}|C_-\rangle$  with real  $\beta(t_f)$ . Thus

$$P_- \approx 1 - \mu^2 \left| \int_0^{t_f} dt \langle \phi_-(t) | e^{-iR_-} H_1(t) e^{iR_+} | \phi_+(t) \rangle \right|^2.$$

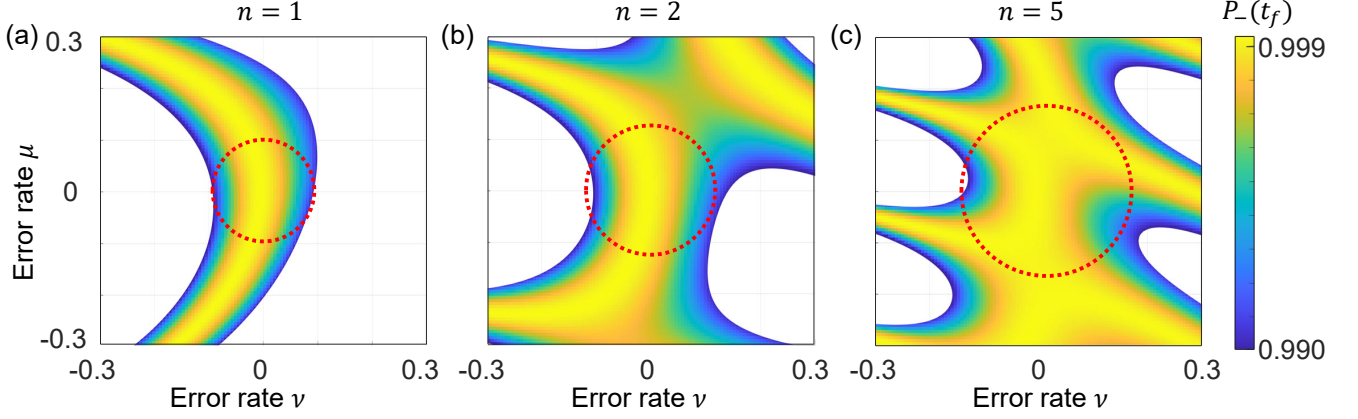


FIG. 6. Population of the odd cat state  $|C_- \rangle$  at time  $t_f$  versus parameter imperfections in  $\epsilon$  (with error rate  $\mu$ ) and  $E_J$  (with error rate  $\nu$ ). Parameters are the same as those in Fig. 5.

Substituting the above expression into the Eq. (25), we can obtain the systematic error sensitivity

$$q_s = \left| \int_0^{t_f} dt \langle \phi_-(t) | e^{-iR_-} H_1(t) e^{iR_+} | \phi_+(t) \rangle \right|^2 = \frac{1}{4} \left| \int_0^{t_f} e^{2iR_+} \Omega_R \left( -\cos^2 \frac{\gamma}{2} e^{2i\beta} + \sin^2 \frac{\gamma}{2} \right) dt \right|^2, \quad (27)$$

From Sec. III, we know that when  $\beta$  approaches  $(n + 1/2)\pi$ , we have  $e^{2i\beta} \rightarrow -1$  and  $\Omega_R(t) = \dot{\gamma}/\sin\beta \simeq -\dot{\gamma}$ . Therefore,  $q_s$  can be approximated as

$$q_s \simeq \frac{1}{4} \left| \int_0^{t_f} \dot{\gamma} dt \right|^2 = \frac{\pi^2}{4}. \quad (28)$$

The relationship between the population  $P_-$  and the systematic error parameter  $\mu$  is shown by the green dashed-dotted curve in Fig. 4. A deviation rate of  $\mu = \pm 0.1$  can lead to an infidelity about 2.5%, which is small but causes significant influence in quantum error correction.

## V. OPTIMAL PROTOCOL

Generally speaking, the two-level Hamiltonian for an optimal control protocol [45] takes the following form:

$$H_{\text{opt}} = \frac{1}{2} \begin{pmatrix} \Delta & \text{Re}[\Omega] - i\text{Im}[\Omega] \\ \text{Re}[\Omega] + i\text{Im}[\Omega] & -\Delta \end{pmatrix}, \quad (29)$$

where  $\text{Re}[*]$  and  $\text{Im}[*]$  denote the real and imaginary parts of the parameter  $*$ , respectively. The derivative of the Lewis-Riesenfeld phases can be obtained through computation

$$\dot{R}_{\pm} = \pm \frac{1}{2\sin\gamma} (\cos\beta \text{Re}[\Omega] - \sin\beta \text{Im}[\Omega]). \quad (30)$$

Using the derivations in Sec. III, we can obtain the expressions for  $\text{Re}[\Omega]$ ,  $\text{Im}[\Omega]$ , and  $\Delta$  as

$$\begin{aligned} \text{Re}[\Omega] &= \cos\beta \sin\gamma \dot{R}_+ + \sin\beta \dot{R}_+, \\ \text{Im}[\Omega] &= -\sin\beta \sin\gamma \dot{R}_+ + \cos\beta \dot{R}_+, \\ \Delta &= \cos\gamma \dot{R}_+ - \dot{\beta}. \end{aligned} \quad (31)$$

For the Hamiltonian  $H_{\text{opt}}$  in Eq. (29), we can derive a new expression for the systematic error sensitivity

$$q_s = \left| \int_0^{t_f} dt \langle \psi_-(t) | H_1(t) | \psi_+(t) \rangle \right|^2 = \frac{1}{4} \left| \int_0^{t_f} dt \left[ e^{2iR_+} \frac{d}{dt} (\cos\gamma \sin\gamma) + e^{2iR_+} \dot{\gamma} \right] \right|^2. \quad (32)$$

Note that the boundary values  $\gamma(0) = \pi$  and  $\gamma(t_f) = 0$ , the expression can be further simplified to

$$q_s = \left| \int_0^{t_f} e^{2iR_+} \dot{\gamma} \sin^2\gamma dt \right|^2. \quad (33)$$

In the special case where  $R_+$  does not vary with time (as in Sec. IV where  $R_+$  is a constant), we obtain  $q_s = \pi^2/4$ .

To make the systematic error sensitivity  $q_s = 0$ , we consider the case where  $R_+$  varies with time, e.g.,

$$R_+(t) = \frac{n}{2} (2\gamma - \sin 2\gamma), \quad (n = 1, 2, 3, \dots), \quad (34)$$

for  $R_+(t)$  in the above expression, we have

$$q_s = \frac{\sin^2(n\pi)}{4n^2}, \quad (35)$$

so, we have  $q_s = 0$  when  $n \neq 0$ . Note that in the limit of  $n \rightarrow 0$ , we obtain  $q_s \rightarrow \pi^2/4$ , which is consistent with the previous statement below Eq. (27). In this case, the expressions for  $\Omega$  and  $\Delta$  are as follows

$$\begin{aligned} \text{Re}[\Omega] &= (4n \cos\beta \sin^3\gamma + \sin\beta) \dot{\gamma}, \\ \text{Im}[\Omega] &= (-4n \sin\beta \sin^3\gamma + \cos\beta) \dot{\gamma}, \\ \Delta &= 4n \dot{\gamma} \cos\gamma \sin^2\gamma - \dot{\beta}. \end{aligned} \quad (36)$$

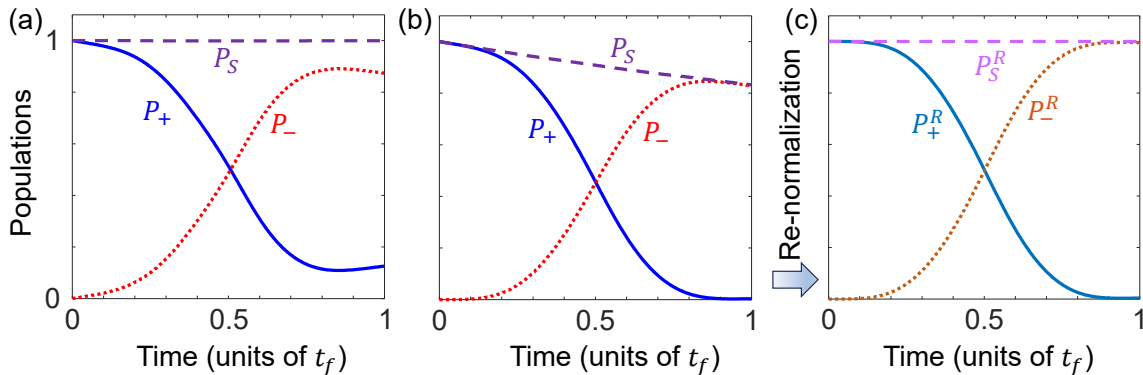


FIG. 7. Population inversion in the presence of (a) single-photon loss and (b) pure dephasing. (c) Re-normalized state population of the system in the presence of pure dephasing. We choose the optimized protocol with  $n = 1$  and the total evolution time  $t_f = 5/K$ . The single-photon loss and pure dephasing rates are  $\kappa = \kappa^\phi = 0.01K$ .

For  $\Omega$  in Eq. (31) to be equivalent with  $\Omega_R$  in Eq. (10), we need to set  $\text{Im}[\Omega] = 0$ , resulting in

$$\cot \beta = 4n \sin^3 \gamma. \quad (37)$$

Then, taking this condition in Eq. (37) and the boundary condition in Eq. (19) and into account, we can redesign the parameters  $\gamma$  and  $\beta$ . For instance, we can still use the polynomial expression in Eq. (20) for  $\gamma$ , then we can obtain new  $\beta$ , as shown at Fig. 5(a). Accordingly,  $\Omega$  and  $\Delta$  can be calculated by Eq. (36), so we can obtain  $E_J$  and  $\epsilon$ , which are shown in Fig. 5(b) and Fig. 5(c), respectively.

Using these optimized parameters, our protocol becomes insensitive to systematic error in the single photon drive (See the blue-solid, red-dashed, and purple-dotted curves in Fig. 4). As can be seen in Fig. 4, the systematic error sensitivity can be significantly reduced by increase  $n$ . For  $n = 5$ , a deviation with  $\mu = \pm 0.3$  in the parameter  $\epsilon$  only leads to a decrease of 0.01% in the final population  $P_-(t_f)$ , resulting in an optimally robust population inversion. Noting that the maximums of  $|\epsilon|$  and  $|E_J|$  increase when  $n$  increases [see Figs. 5(b) and (c)], a longer operator time  $t_f$  is needed to satisfy  $|\epsilon|, |E_J| \ll \omega_{\text{gap}}$  for large  $n$ . Figure 5(d) shows the time-dependent population  $P_-(t)$ . It is found that increasing  $n$  does not change the instantaneous population  $P_-(t)$ . This is because the instantaneous population  $P_-(t)$  is determined by the parameter  $\gamma$ , which keeps the same for different  $n$ .

The above discussion focuses on improving the robustness against parameter imperfections in  $\epsilon$ . When parameter imperfections appear in  $E_J$ , our protocol can also achieve a robust population inversion as shown in Fig. 6. In this case, we consider an additional disturbed Hamiltonian

$$H_2 = -\nu E_J(t) \{D[i\varphi_a \exp(i\omega_c t)] + \text{H.c.}\} / 2, \quad (38)$$

where  $\nu$  denotes the error rate. The population of the target state  $|C_-\rangle$  can still reach  $\geq 99\%$  when the error

rate is  $\nu = \pm 0.1$  via our protocol with  $n = 1$  [see Fig. 6(a)]. Increasing the value of  $n$  can further improve the robustness against systematic errors. However, to achieve such an optimal robustness, an increase in the total evolution time is needed as discussed above. This becomes a defect of the protocol when considering decoherence. Therefore, for simplicity, we use the pulse with  $n = 1$  in the following numerical simulations.

## VI. DECOHERENCE

For the resonator, we consider two types of noise: single-photon loss and pure dephasing. The system dynamics are described by the Lindblad master equation [1, 2]

$$\dot{\rho} = -i[H_{\text{Kerr}}, \rho] + \kappa \mathcal{D}[a]\rho + \kappa^\phi \mathcal{D}[a^\dagger a]\rho, \quad (39)$$

where

$$\mathcal{D}[o]\rho = o\rho o^\dagger - \frac{1}{2}(o^\dagger o\rho + \rho o^\dagger o)$$

is the standard Lindblad superoperator,  $\kappa$  is the single-photon dissipation rate, and  $\kappa^\phi$  is the pure dephasing rate. Projecting the whole system onto the cat-state subspace, we can obtain

$$\begin{aligned} \dot{\rho}_{\text{eff}} \approx & -i[H_{\text{eff}}, \rho_{\text{eff}}] \\ & + \kappa |\alpha|^2 \mathcal{D} \left[ \frac{A + A^{-1}}{2} \sigma_x + \frac{A - A^{-1}}{2} \sigma_y \right] \rho_{\text{eff}} \\ & + \kappa^\phi |\alpha|^4 \mathcal{D} \left[ \frac{A^2 + A^{-2}}{2} \mathbb{1} - \frac{A^2 - A^{-2}}{2} \sigma_z \right] \rho_{\text{eff}}, \end{aligned} \quad (40)$$

where  $A = \tanh |\alpha|^2$  and  $\mathbb{1} = |C_+\rangle\langle C_+| + |C_-\rangle\langle C_-|$  is the unit matrix in the cat-state subspace. For large  $\alpha$ ,  $\sigma_y$

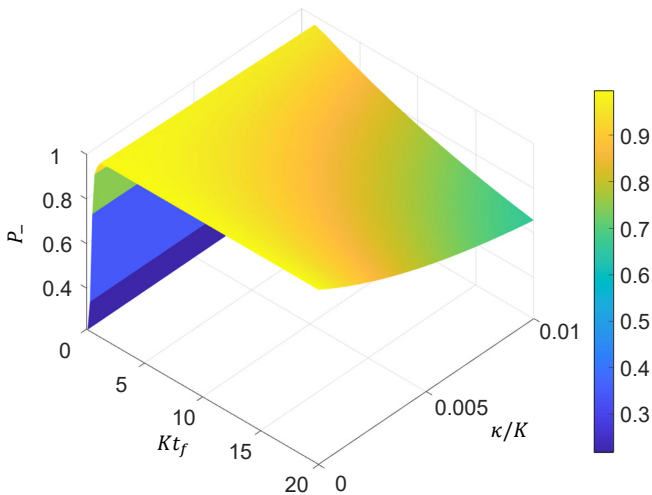


FIG. 8. Population  $P_-$  versus the total evolution time  $t_f$  and single-photon loss rate  $\kappa$ . We choose the optimized protocol with  $n = 1$  and assume pure dephasing  $\kappa^\phi = 0$ .

and  $\sigma_z$  terms are exponentially suppressed, resulting in

$$\dot{\rho}_{\text{eff}} \approx -i[H_{\text{eff}}, \rho_{\text{eff}}] + \kappa|\alpha|^2\mathcal{D}[\sigma_x]\rho_{\text{eff}}, \quad (41)$$

i.e., leaving only the bit-flipping error. This is demonstrated in Fig. 7(a), which shows that single-photon loss causes bit-flipping error but no leakage. The sum of populations

$$P_S = P_+ + P_-, \quad (42)$$

in the cat-state subspace remains unchanged in the presence of single-photon loss.

According to Eq (41), pure dephasing has no influence on the dynamics in the cat-state subspace. However, pure dephasing can cause leakage out of the cat-state subspace [see Fig. 7(b)] because

$$a^\dagger a |\pm \alpha\rangle = |\alpha|^2 |\pm \alpha\rangle \pm \alpha D(\pm \alpha) |1\rangle. \quad (43)$$

This leakage probability is proportional to  $|\kappa\alpha/\omega_{\text{gap}}|^2$  [19, 20]. The total population in the cat-state subspace reduces obviously as shown in the figure. To further analyze the influence of pure dephasing on the dynamics in the cat-state subspace, we define

$$P_+^R = \frac{P_+}{P_+ + P_-}, \quad \text{and} \quad P_-^R = \frac{P_-}{P_+ + P_-}, \quad (44)$$

to be the normalized state populations in the cat-state subspace and display them in Fig. 7(c). Obviously, a perfect population inversion is still possible in the presence of pure dephasing.

We also investigate the influence of total evolution time  $t_f$  on the protocol. As shown in Fig. 8, an evolution time of  $t_f \simeq 1/K$  is enough for our protocol to achieve the high-fidelity population inversion in the

presence of decoherence. For instance, when  $t_f = 1.1/K$  and  $\kappa = 0.01K$ , the final population can reach  $P_- \simeq 96\%$ , demonstrating the effectiveness of our optimized population inversion protocol.

## VII. DISCUSSION AND CONCLUSIONS

The proposed protocol is possible to be realized in superconducting circuits [9, 27, 47–54], especially the platforms with 3-dimension cavities [11, 12, 23, 55–58]. This is because that the 3-dimension cavities can provide a relatively long coherent time (extending to microseconds) for photonic qubits [11, 12]. Cat-state qubits also belong to a larger family of bosonic qubits, most of which have been realized with 3-dimension cavities [11, 12]. To be specific, the Kerr nonlinearity and the two-photon drive can be respectively realized by the Josephson junction (transmon) nonlinearity and four-wave mixing [19, 59–62]. The control Hamiltonian in Eq. (5) is possible to realize by considering the Kerr-nonlinear mode coupled capacitively to a Josephson junction and assuming that other modes (including the junction mode) are never excited [46]. Following the first cat-state qubit experiment, we can consider the experimental parameters  $K/2\pi = 6.7$  MHz,  $\kappa/2\pi \simeq 0.01$  MHz, and  $\kappa^\phi/2\pi \simeq 0.045$  MHz. With these parameters and  $t_f = 1.1/K \simeq 26$  ns, the final population of the target state is  $P_-(t_f) \simeq 95\%$  in the presence of parameter imperfection with  $\mu = \nu = 0.1$  and decoherence. When re-normalizing the state populations in the cat-state subspace using Eq. (44), the normalized state population of the odd cat state  $|\mathcal{C}_-\rangle$  becomes  $P_-^R \simeq 98.6\%$ .

In conclusion, we have investigated a feasible control method to obtain the optimally robust shortcut to population inversion in cat-state qubits. Focusing on the Kerr-cat qubit, which is realized by parametrically driving a Kerr-nonlinear resonator, we have constructed shortcuts to adiabatic passages and minimized the systemic error sensitivity based on the invariant-based reverse engineering. Future work will involve extending our results to other logic qubits and the multi-qubit cases. The existence of a set of optimal solutions for systematic errors also opens the way to further optimization with respect to other error-correcting qubits.

## ACKNOWLEDGMENTS

Y.-H.C. is supported by the National Natural Science Foundation of China under Grant No. 12304390 and the Project from Fuzhou University under Grant XRC-23051. Y.X. is supported by the National Natural Science Foundation of China under Grant No. 11575045, the Natural Science Funds for Distinguished Young Scholar of Fujian Province under Grant 2020J06011 and Project from Fuzhou University under Grant JG202001-2.

- [1] M. O. Scully and M. S. Zubairy, *Quantum Optics* (Cambridge University Press, Cambridge, England, 1997).
- [2] Girish S. Agarwal, *Quantum Optics* (Cambridge University Press, Cambridge, England, 2012).
- [3] J. D. Hidary, *Quantum Computing: An Applied Approach* (Springer, Berlin, 2019).
- [4] R. J. Lipton and K. W. Regan, *Introduction to Quantum Algorithms via Linear Algebra* (The MIT Press, Cambridge, 2021).
- [5] A. F. Kockum and F. Nori, “Quantum bits with Josephson junctions,” in *Fundamentals and Frontiers of the Josephson Effect*, Vol. 286, edited by F. Tafuri (Springer, Berlin, 2019) Chap. 17, pp. 703–741.
- [6] P. W. Shor, “Scheme for reducing decoherence in quantum computer memory,” *Phys. Rev. A* **52**, R2493–R2496 (1995).
- [7] A. Steane, “Multiple-particle interference and quantum error correction,” *Proc. Roy. Soc. Lond. A* **452**, 2551–2577 (1996).
- [8] D. A. Lidar and T. A. Brun, eds., *Quantum Error Correction* (Cambridge Univ. Press, New York, 2013).
- [9] M. Kjaergaard, M. E. Schwartz, J. Braumüller, P. Krantz, J. I.-J. Wang, S. Gustavsson, and W. D. Oliver, “Superconducting qubits: Current state of play,” *Ann. Rev. Cond. Matt. Phys.* **11**, 369–395 (2020).
- [10] A. Y. Kitaev, “Fault-tolerant quantum computation by anyons,” *Ann. Phys.* **303**, 2–30 (2003).
- [11] W. Cai, Y. Ma, W. Wang, C.-L. Zou, and L. Sun, “Bosonic quantum error correction codes in superconducting quantum circuits,” *Fund. Res.* **1**, 50–67 (2021).
- [12] W.-L. Ma, S. Puri, R. J. Schoelkopf, M. H. Devoret, S. M. Girvin, and L. Jiang, “Quantum control of bosonic modes with superconducting circuits,” *Sci. Bull.* **66**, 1789–1805 (2021).
- [13] T. C. Ralph, A. Gilchrist, G. J. Milburn, W. J. Munro, and S. Glancy, “Quantum computation with optical coherent states,” *Phys. Rev. A* **68**, 042319 (2003).
- [14] M. Mirrahimi, Z. Leghtas, V. V. Albert, S. Touzard, R. J. Schoelkopf, L. Jiang, and M. H. Devoret, “Dynamically protected cat-qubits: a new paradigm for universal quantum computation,” *New J. Phys.* **16**, 045014 (2014).
- [15] M. Mirrahimi, “Cat-qubits for quantum computation,” *Comptes Rendus Phys.* **17**, 778–787 (2016).
- [16] C. Chamberland, K. Noh, P. Arrangoiz-Arriola, E. T. Campbell, C. T. Hann, J. Iverson, H. Putterman, T. C. Bohdanowicz, S. T. Flammia, A. Keller, G. Refael, J. Preskill, L. Jiang, A. H. Safavi-Naeini, O. Painter, and F. G. S. L. Brandão, “Building a fault-tolerant quantum computer using concatenated cat codes,” *PRX Quantum* **3**, 010329 (2022).
- [17] P. Aliferis and J. Preskill, “Fault-tolerant quantum computation against biased noise,” *Phys. Rev. A* **78**, 052331 (2008).
- [18] S. Puri, S. Boutin, and A. Blais, “Engineering the quantum states of light in a Kerr-nonlinear resonator by two-photon driving,” *npj Quantum Inf.* **3**, 18 (2017).
- [19] S. Puri, A. Grimm, P. Campagne-Ibarcq, A. Eickbusch, K. Noh, G. Roberts, L. Jiang, M. Mirrahimi, M. H. Devoret, and S. M. Girvin, “Stabilized cat in a driven nonlinear cavity: A fault-tolerant error syndrome detector,” *Phys. Rev. X* **9**, 041009 (2019).
- [20] S. Puri, L. St-Jean, J. A. Gross, A. Grimm, N. E. Frattini, P. S. Iyer, A. Krishna, S. Touzard, L. Jiang, A. Blais, S. T. Flammia, and S. M. Girvin, “Bias-preserving gates with stabilized cat qubits,” *Sci. Adv.* **6**, eaay5901 (2020).
- [21] V. V. Albert, C. Shu, S. Krastanov, C. Shen, R.-B. Liu, Z.-B. Yang, R. J. Schoelkopf, M. Mirrahimi, M. H. Devoret, and L. Jiang, “Holonomic quantum control with continuous variable systems,” *Phys. Rev. Lett.* **116**, 140502 (2016).
- [22] V. V. Albert, S. O. Mundhada, A. Grimm, S. Touzard, M. H. Devoret, and L. Jiang, “Pair-cat codes: autonomous error-correction with low-order nonlinearity,” *Quantum Sci. Tech.* **4**, 035007 (2019).
- [23] W. Cai, J. Han, L. Hu, Y. Ma, X. Mu, W. Wang, Y. Xu, Z. Hua, H. Wang, Y. P. Song, J.-N. Zhang, C.-L. Zou, and L. Sun, “High-efficiency arbitrary quantum operation on a high-dimensional quantum system,” *Phys. Rev. Lett.* **127**, 090504 (2021).
- [24] Y.-H. Chen, W. Qin, X. Wang, A. Miranowicz, and F. Nori, “Shortcuts to adiabaticity for the quantum Rabi model: Efficient generation of giant entangled cat states via parametric amplification,” *Phys. Rev. Lett.* **126**, 023602 (2021).
- [25] Y.-H. Chen, R. Stassi, W. Qin, A. Miranowicz, and F. Nori, “Fault-tolerant multiqubit geometric entangling gates using photonic cat-state qubits,” *Phys. Rev. Appl.* **18**, 024076 (2022).
- [26] Y.-H. Chen, Z.-C. Shi, F. Nori, and Y. Xia, “Error-tolerant amplification and simulation of the ultrastrong-coupling quantum Rabi model,” *Phys. Rev. Lett.* **133**, 033603 (2024).
- [27] A. Grimm, N. E. Frattini, S. Puri, S. O. Mundhada, S. Touzard, M. Mirrahimi, S. M. Girvin, S. Shankar, and M. H. Devoret, “Stabilization and operation of a Kerr-cat qubit,” *Nature (London)* **584**, 205–209 (2020).
- [28] A. S. Darmawan, B. J. Brown, A. L. Grimsmo, D. K. Tuckett, and S. Puri, “Practical quantum error correction with the XZZX code and kerr-cat qubits,” *PRX Quantum* **2**, 030345 (2021).
- [29] Q. Xu, H. Putterman, J. K. Iverson, K. Noh, O. J. Painter, F. G. S. L. Brandao, and L. Jiang, *Quantum Computing, Communication, and Simulation II*, edited by P. R. Hemmer and A. L. Migdall (SPIE, 2022).
- [30] Y.-H. Kang, Y.-H. Chen, X. Wang, J. Song, Y. Xia, A. Miranowicz, S.-B. Zheng, and F. Nori, “Nonadiabatic geometric quantum computation with cat-state qubits via invariant-based reverse engineering,” *Phys. Rev. Res.* **4**, 013233 (2022).
- [31] Z. Wang, M. Pechal, E. A. Wollack, P. Arrangoiz-Arriola, M. Gao, N. R. Lee, and A. H. Safavi-Naeini, “Quantum dynamics of a few-photon parametric oscillator,” *Phys. Rev. X* **9**, 021049 (2019).
- [32] X. Chen, I. Lizuain, A. Ruschhaupt, D. Guéry-Odelin, and J. G. Muga, “Shortcut to adiabatic passage in two- and three-level atoms,” *Phys. Rev. Lett.* **105**, 123003 (2010).
- [33] S. Campbell *et al.*, “Shortcut to adiabaticity in the Lipkin-Meshkov-Glick model,” *Phys. Rev. Lett.* **114**,



- 177206 (2015).
- [34] E. Torrontegui *et al.*, “Shortcuts to adiabaticity,” in *Adv. Atom. Mol. Opt. Phys.* (Elsevier, 2013) p. 117–169.
- [35] B. B. Zhou *et al.*, “Accelerated quantum control using superadiabatic dynamics in a solid-state lambda system,” *Nature Physics* **13**, 330–334 (2016).
- [36] Y.-X. Du *et al.*, “Experimental realization of stimulated Raman shortcut-to-adiabatic passage with cold atoms,” *Nat. Commun.* **7**, 12479 (2016).
- [37] T. Hatomura, “Shortcuts to adiabatic cat-state generation in bosonic Josephson junctions,” *New J. Phys.* **20**, 015010 (2018).
- [38] S. Ibáñez, X. Chen, E. Torrontegui, J. G. Muga, and A. Ruschhaupt, “Multiple Schrödinger pictures and dynamics in shortcuts to adiabaticity,” *Phys. Rev. Lett.* **109**, 100403 (2012).
- [39] D. Guéry-Odelin, A. Ruschhaupt, A. Kiely, E. Torrontegui, S. Martínez-Garaot, and J. G. Muga, “Shortcuts to adiabaticity: Concepts, methods, and applications,” *Rev. Mod. Phys.* **91**, 045001 (2019).
- [40] K. Funo *et al.*, “Shortcuts to adiabatic pumping in classical stochastic systems,” *Phys. Rev. Lett.* **124**, 150603 (2020).
- [41] O. Abah, R. Puebla, and M. Paternostro, “Quantum state engineering by shortcuts to adiabaticity in interacting spin-boson systems,” *Phys. Rev. Lett.* **124**, 180401 (2020).
- [42] K. Takahashi and A. del Campo, “Shortcuts to adiabaticity in Krylov space,” *Phys. Rev. X* **14**, 011032 (2024).
- [43] H. R. Lewis and W. B. Riesenfeld, “An exact quantum theory of the time-dependent harmonic oscillator and of a charged particle in a time-dependent electromagnetic field,” *J. Math. Phys.* **10**, 1458–1473 (1969).
- [44] X. Chen, E. Torrontegui, and J. G. Muga, “Lewis-Riesenfeld invariants and transitionless quantum driving,” *Phys. Rev. A* **83**, 062116 (2011).
- [45] A. Ruschhaupt, X. Chen, D. Alonso, and J. G. Muga, “Optimally robust shortcuts to population inversion in two-level quantum systems,” *New J. Phys.* **14**, 093040 (2012).
- [46] J. Cohen, W. C. Smith, M. H. Devoret, and M. Mirrahimi, “Degeneracy-preserving quantum nondemolition measurement of parity-type observables for cat qubits,” *Phys. Rev. Lett.* **119**, 060503 (2017).
- [47] J. Koch, T. M. Yu, J. Gambetta, A. A. Houck, D. I. Schuster, J. Majer, A. Blais, M. H. Devoret, S. M. Girvin, and R. J. Schoelkopf, “Charge-insensitive qubit design derived from the cooper pair box,” *Phys. Rev. A* **76**, 042319 (2007).
- [48] J. Q. You, X. Hu, S. Ashhab, and F. Nori, “Low-decoherence flux qubit,” *Phys. Rev. B* **75**, 140515(R) (2007).
- [49] E. Flurin, N. Roch, J. D. Pillet, F. Mallet, and B. Huard, “Superconducting quantum node for entanglement and storage of microwave radiation,” *Phys. Rev. Lett.* **114**, 090503 (2015).
- [50] W. Wustmann and V. Shumeiko, “Parametric resonance in tunable superconducting cavities,” *Phys. Rev. B* **87**, 184501 (2013).
- [51] X. Gu, A. F. Kockum, A. Miranowicz, Y. x. Liu, and F. Nori, “Microwave photonics with superconducting quantum circuits,” *Phys. Rep.* **718-719**, 1–102 (2017).
- [52] P. Krantz, M. Kjaergaard, F. Yan, T. P. Orlando, S. Gustavsson, and W. D. Oliver, “A quantum engineer's guide to superconducting qubits,” *Appl. Phys. Rev.* **6**, 021318 (2019).
- [53] M. Kjaergaard, M. E. Schwartz, J. Braumüller, P. Krantz, J. I.-J. Wang, S. Gustavsson, and W. D. Oliver, “Superconducting qubits: Current state of play,” *Ann. Rev. Cond. Mat. Phys.* **11**, 369–395 (2020).
- [54] S. Kwon, A. Tomonaga, G. L. Bhai, S. J. Devitt, and J.-S. Tsai, “Gate-based superconducting quantum computing,” *J. Appl. Phys.* **129**, 041102 (2021).
- [55] L. Hu, Y. Ma, W. Cai, X. Mu, Y. Xu, W. Wang, Y. Wu, H. Wang, Y. P. Song, C.-L. Zou, S. M. Girvin, L.-M. Duan, and L. Sun, “Quantum error correction and universal gate set operation on a binomial bosonic logical qubit,” *Nat. Phys.* **15**, 503–508 (2019).
- [56] Y. Xu, Y. Ma, W. Cai, X. Mu, W. Dai, W. Wang, L. Hu, X. Li, J. Han, H. Wang, Y. P. Song, Z.-B. Yang, S.-B. Zheng, and L. Sun, “Demonstration of controlled-phase gates between two error-correctable photonic qubits,” *Phys. Rev. Lett.* **124**, 120501 (2020).
- [57] Z. Wang and others., “An ultra-high gain single-photon transistor in the microwave regime,” *Nat. Commun.* **13** (2022).
- [58] Z. Ni *et al.*, “Beating the break-even point with a discrete-variable-encoded logical qubit,” *Nature (London)* **616**, 56–60 (2023).
- [59] Y.-H. Chen, W. Qin, and F. Nori, “Fast and high-fidelity generation of steady-state entanglement using pulse modulation and parametric amplification,” *Phys. Rev. A* **100**, 012339 (2019).
- [60] W. Qin, V. Macrì, A. Miranowicz, S. Savasta, and F. Nori, “Emission of photon pairs by mechanical stimulation of the squeezed vacuum,” *Phys. Rev. A* **100**, 062501 (2019).
- [61] W. Qin, Y.-H. Chen, X. Wang, A. Miranowicz, and F. Nori, “Strong spin squeezing induced by weak squeezing of light inside a cavity,” *Nanophotonics* **9**, 4853–4868 (2020).
- [62] W. Qin, A. Miranowicz, H. Jing, and F. Nori, “Generating long-lived macroscopically distinct superposition states in atomic ensembles,” *Phys. Rev. Lett.* **127**, 093602 (2021).